Chapter 4

PROTOTYPE DESIGN

4.1 Introduction

The previous two chapters have described the physics of zero-field paramagnetic resonance with little reference to the experimental techniques used to measure zero-field magnetic resonance, or the practical design of a solid-state atomic frequency standard. The most important articles which described zero-field electron magnetic resonance spectrometer designs are those by Bramley *et al.* [1,2,3,4]. Some early spectrometers detect the change in attenuation or phase along a non-resonant transmission line containing the paramagnetic sample, however, a resonant design using a tunable resonator is much more sensitive. While apparently a simple problem, designing a broadly tunable, high-Q electrical resonator is non-trivial. One solution is to use a mechanically tuned "loop-gap" resonator, as will be described in this chapter. The loop-gap resonator is especially effective in paramagnetic resonance experiments because of the combination of high-Q and small volume.

The loop-gap resonator is used in the proof-of-concept because of the broad tuning range which is useful for measuring different samples and features of the spectrum. For a prototype solid-state atomic frequency standard, smaller resonators such as a coaxial resonator made from magnesium oxide ceramic can be used with varactor tuning over a few percent bandwidth.

As described in Chapter 2, paramagnetic resonance may be detected as a change in the resonant frequency and quality factor of an electrical resonator which contains a paramagnetic sample. The interaction between the paramagnetic resonance and the resonant magnetic fields cause a perturbation to both the frequency and losses of the

electrical resonator. A diagram of the prototype spectrometer is illustrated in Figure 4.1. The frequency discriminator consists of the electrical resonator, phase detector, hybrid coupler or power splitter, and phase adjuster.

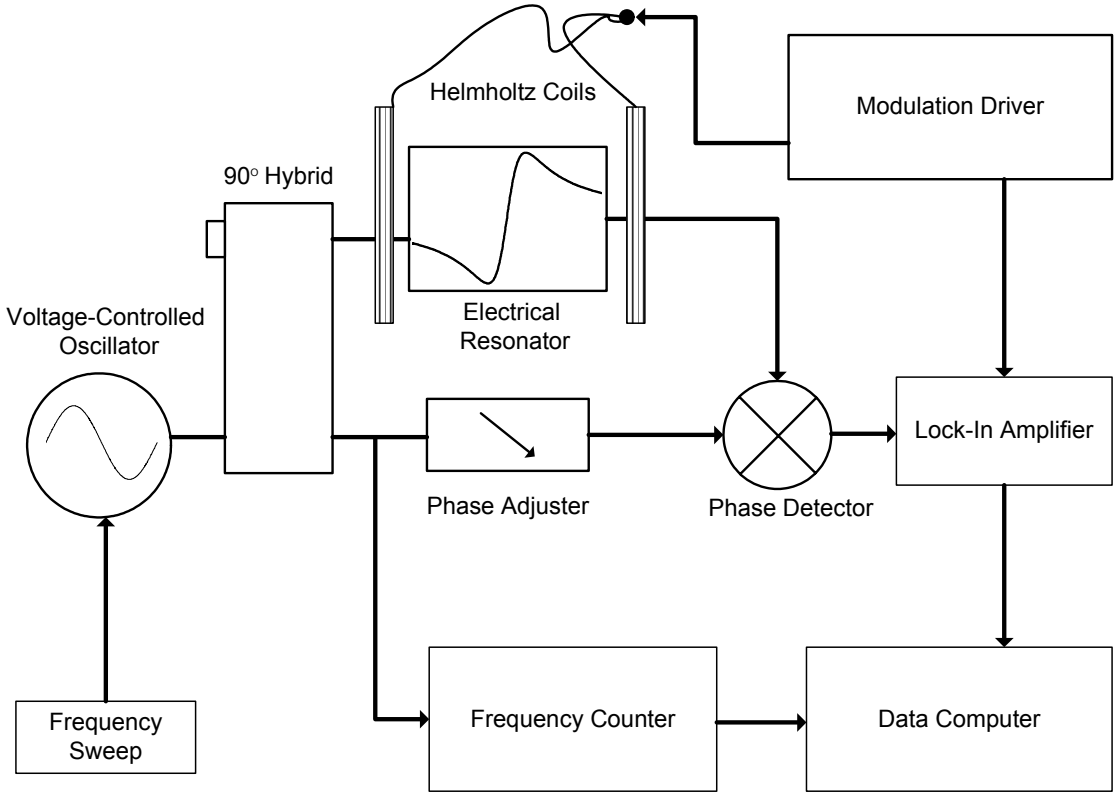

Figure 4.1: Zero-Field Electron Magnetic Resonance Spectrometer

Fluctuations or modulation of the resonant frequency of the electrical resonator are demodulated by the frequency discriminator to generate a voltage proportional to the frequency deviation. Because the magnetic resonance signals are small, lock-in detection is necessary to isolate the magnetic resonance signal. The Helmholtz coils shown in Figure 4.0 apply an audio magnetic field to the paramagnetic sample inside the electrical resonator, which modulates the magnetic resonance signal because of the Zeeman shift (Chapter 2). The resulting frequency modulation of the electrical resonator is demodulated using the frequency discriminator and detected with the lock-in amplifier.

There are two key features of the zero-field magnetic resonance spectrometer design. The first is the tunable loop-gap resonator mentioned above, which is essential for adequate sensitivity (Figure 4.2):

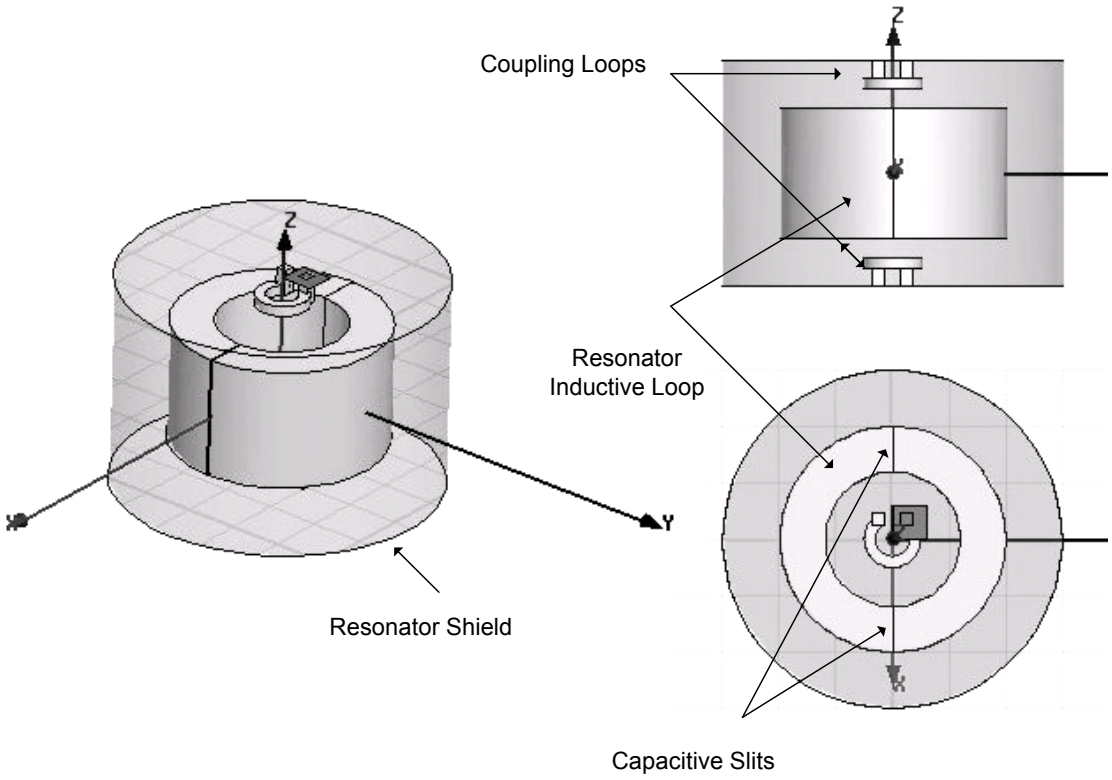

Figure 4.2: Shielded Loop-Gap Resonator: Perspective, Side and Top View

The loop-gap resonator consists of an inductive loop with two narrow capacitive slits, which form a lumped LC resonant circuit. The resonator is coupled via the mutual inductance between the small coupling loops and the resonator inductive loop Figure 4.2.

The second is to use "bidirectional" magnetic field modulation, shown in the upper waveform of Figure. 4.3. This modulation scheme has the advantage of reducing spurious modulation pickup by 50 dB or more, compared to simple ON/OFF modulation. The response of the electron spin resonance transitions is symmetric to the inversion of the

magnetic field, and the desired modulation signal is measured at twice the fundamental, driving the lock-in amplifier with the lower waveform shown in Figure. 4.3.

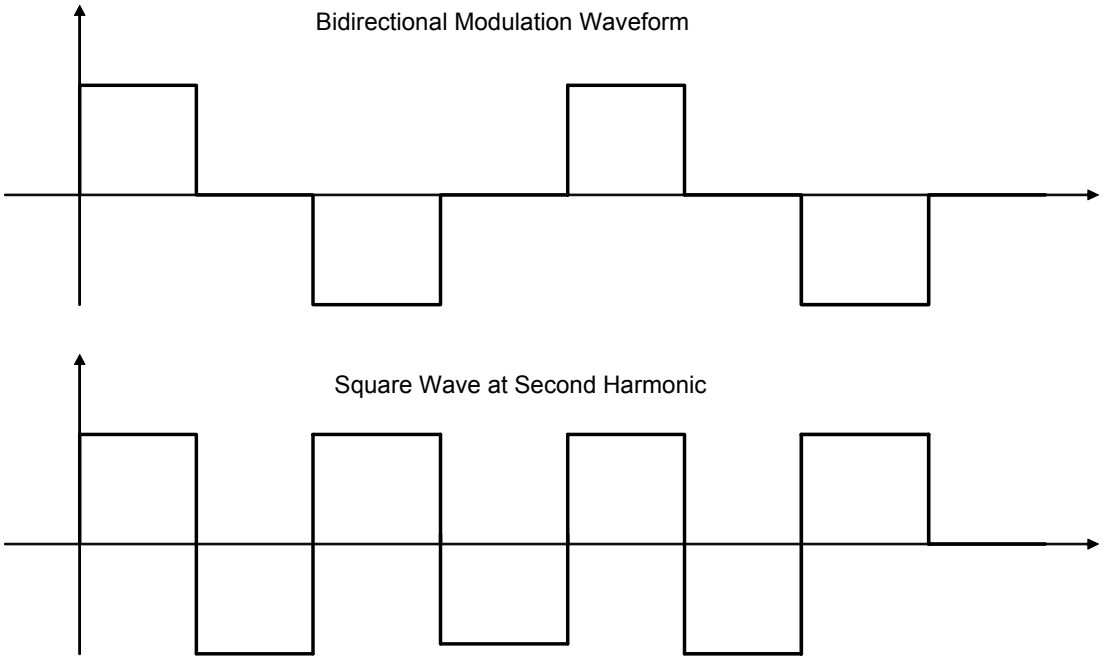

Figure 4.3: Audio Modulation Waveform and Lock-In Multiplier Waveform

The radio-frequency signal processing detects the frequency modulation of the electrical resonator containing the paramagnetic sample. Most electron spin resonance spectrometers detect the magnetic resonance absorption signal (*i.e.*, change in the Q of the resonator) rather than dispersion (*i.e.*, change in the frequency of the electrical resonator), and measure the reflection from a critically coupled cavity using a circulator. Frequency discriminators can be very sensitive, limited by thermal noise even at large RF carrier powers, and as such are a type of "null instrument" [6,7]. Fundamentally, the sensitivity of the frequency modulation measurement is limited by the intrinsic frequency fluctuations of the electrical resonator. For example, excessive noise from vibrations, causing random modulation of the electrical resonant frequency, can be a limiting factor in the sensitivity. The noise sources are analyzed in Chapter 5.

This chapter contains very specific details on the construction of the loop-gap resonator and electronic system, to provide a "recipe" for future researchers, and a list of materials and suppliers in the appendix.

4.2 Tunable Loop-Gap Resonator Design

There are many examples of loop-gap resonators in the electron spin resonance literature [8,9,10,11,12.] The use of loop-gap resonators in place of waveguide cavity resonators is becoming more popular, especially for experiments on aqueous samples where L- and S-band spectrometers have less dielectric loss than at X-band.

(a) Loop-gap resonator

As previously discussed, Figure 4.2 depicts an electrical resonator. The loop-gap resonator comprises an inductive ring with one or more capacitive slits. In the prototype, there are two capacitive slits which allows for mechanical tuning over more than one octave by adjusting the capacitive gap using a flexure stage. The technique realizes a resonator which have both high-Q (in the range of 500) and wideband tuning.

The resonant frequency is approximately equal to:

$$2\pi\nu = \frac{1}{(LC)^{1/2}} = \frac{1}{r} n^{1/2} \left(\frac{t}{W}\right)^{1/2} \left(\frac{1}{\pi\varepsilon\mu_0}\right)^{1/2} \tag{4.1}$$

Equation 4.1 does not account for fringing fields; more accurate semi-empirical equations are found in the literature [11]. The geometric quantities in the equation are illustrated below (Figure 4.4):

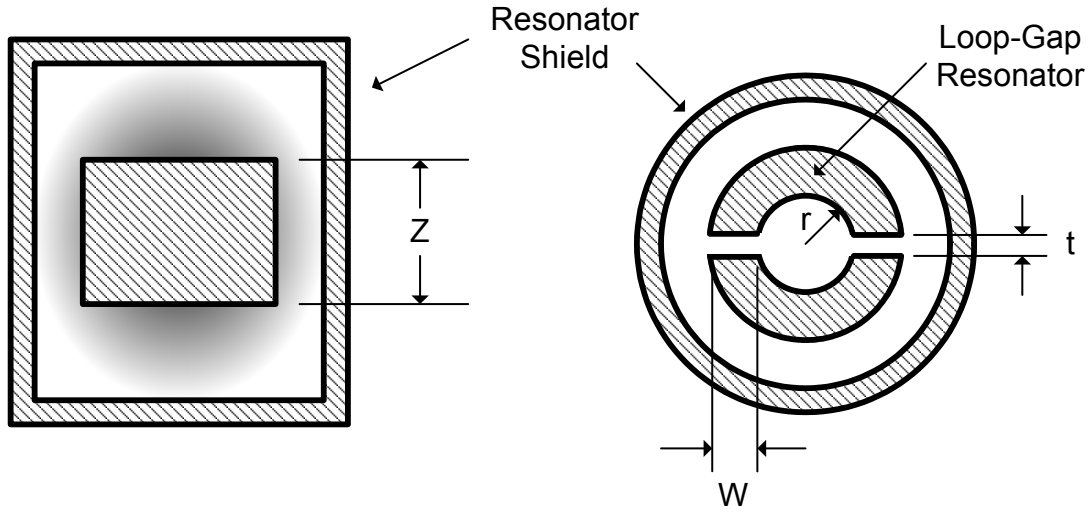

Figure 4.4: Mechanical Dimensions of Loop-Gap Resonator

In the prototype, the resonator height *Z* was approximately 0.5'', the inner radius *r* was 0.3'', the thickness was 0.1'', and the capacitive gap *t* was tuned between 10 microns and 25 microns. The resonant frequency tunes from approximately 1-2 GHz. The prototype dimensions are shown in more detail in the manufacturing drawings (Appendix I). Coupling to the resonator is achieved using coupling loops soldered directly to SMA connectors mounted on the resonator shield. In the prototype, the coupling loops (Figure 4.2) are made from silver plated 18-gauge phosphor bronze wire. The inner diameter of the coupling loops is approximately 4 millimeters. The frequency of the loop-gap resonator can be mechanically tuned over more than one octave by varying the thickness of the two capacitive gaps, and therefore the frequency of the LC resonator.

The center of the loop-gap resonator includes a paramagnetic sample during measurements, which interacts with the RF magnetic field inside the inductive ring. In addition to the advantages of high-Q, small volume, and broad tuning, the RF magnetic field inside the inductive loop is substantially uniform, and therefore, the paramagnetic resonance saturates uniformly at high carrier power.

Minimizing leakage of the RF signal stored in the loop-gap resonator is essential to prevent unwanted mixing between the RF and modulation signals. The best technique is to electroplate the resonator shield (Figure 4.2 and 4.4) of the loop-gap resonator to a thickness of approximately 10 microns, which provides maximum isolation. The audio-frequency magnetic field penetrates this thin layer of metal with very little attenuation, and the RF signal is completely shielded, because the skin-depth is typically much less than 10 microns. Cutting slits in a metal shield to allow the audio magnetic field to penetrate the sample is not a good design because RF isolation is poor.

The loop-gap resonator is tuned by mechanically varying the thickness of the capacitive gaps, using a flexure stage as shown in Figure 4.5:

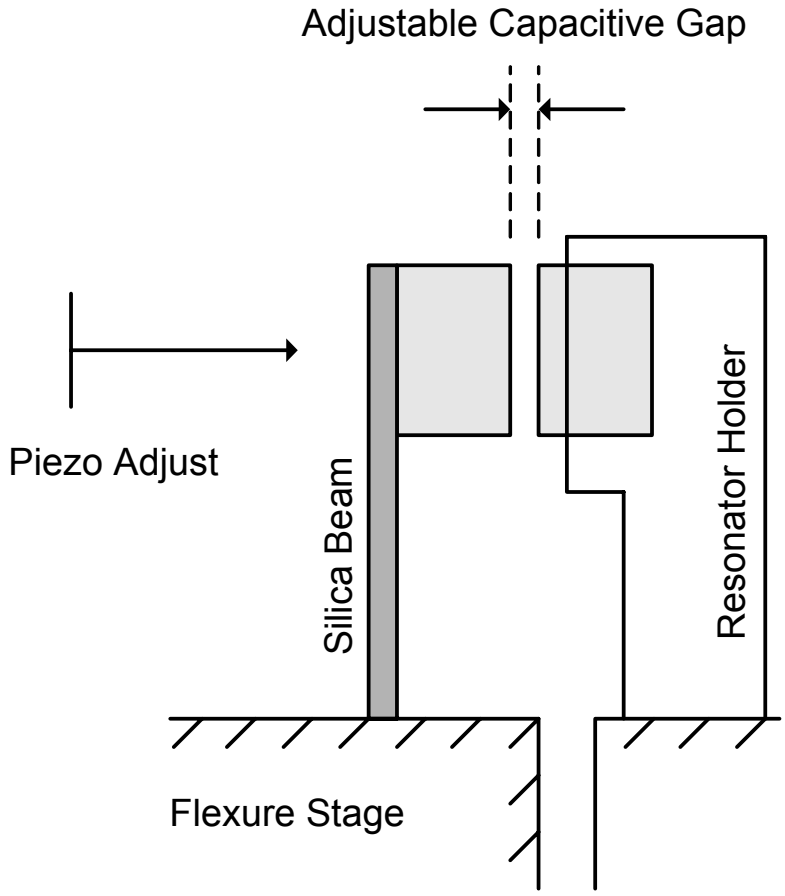

Figure 4.5: Side View of Mechanically Tunable Loop-Gap Resonator

The flexure stage adjusts the capacitance gap between approximately 10 microns and 25 microns, which tunes the resonator from ~ 800 MHz to 2 GHz. The resonator pieces may be coating with insulating material such as parylene to prevent shorting across the gap.

A weakness of the present design is the sensitivity of the cantilevered resonator piece to acoustics and vibrations, which modulate the frequency of the loop-gap resonator. Acoustic pickup of the applied modulation signals is also possible, as vibrations are excited by the Lorentz force between the modulation coils or adjacent wires of a single coil.

Further details of the design of loop-gap resonators are extensively elaborated in the scientific literature on electron spin resonance, see references [8,9,10,11,12]. Other techniques for implementing a multi-octave tunable loop-gap resonator are described in [1,2,3].

4.3 Loop-Gap Resonator Manufacturing

The ideal design for the resonator uses thin plated metal surfaces to provide complete RF isolation without shielding the audio magnetic field. RF leakage is to be avoided to prevent spurious mixing with the modulation signals.

The loop-gap resonator and resonator shield were machined from MACOR™ ceramic. Coupling loops are made from phosphor brass (Figure 4.2). Manufacturing drawings for the design used in the spectrometer prototype are provided in Appendix I, along with the part numbers and manufacturers contact information for the components used in the loop-gap resonator in Appendix II. The ceramic pieces are coated with a conducting layer using a commercial silvering solution (HE-300) obtained from Peacock Laboratories, Inc. (Philadelphia, PA). Cleaning with red rouge prior to silvering (Mc-Master Carr P/N 4783A3) greatly improves the quality of the silvered film. The silvered MACOR pieces were then electroplated to approximately 10 microns silver by Hudson Plating Works, Inc. (Canoga Park, CA). In the first design, a Rexolite® rod was used to position the loop-gap

resonator. However, a silica rod is a better choice because of greater mechanical stability. Custom precision ground silica rods were manufactured by Rayotek Scientific, Inc. (San Diego, CA.) The glass rod is attached to the silvered MACOR piece using a small clamping fixture and a drop of cyanoacetate glue (Superglue). In a further aspect of the design, resonator holders is machined from Rexolite ® (C-Lee Plastics, Inc., Philadelphia, Pennsylvania) (not shown in Fig. 4.2).

The precision flexure stage is used to adjust the resonator capacitive gap, which tuned the resonant frequency. The piezo adjuster was model MDE218 Piezo Adjuster (Elliot Scientific, UK), and the 150V piezo driver was Thorlabs model MDT 694. Noise from the piezo driver must be carefully filtered. It was found that a large electrolytic capacitor (330uF, 150V, Mallory) was an effective noise filter in combination with the 50 Ω output impedance of the piezo driver.

4.4 Frequency Discriminator

The frequency discriminator circuit is simply a mixer adjusted in quadrature with the electrical resonator in one path (Figure 4.6). Important considerations are the isolation of the power divider and the impedance matching of all paths. Reflection from the mixer or mismatch of the loop-gap resonator impedance cause unwanted power and phase variations as the frequency is swept.

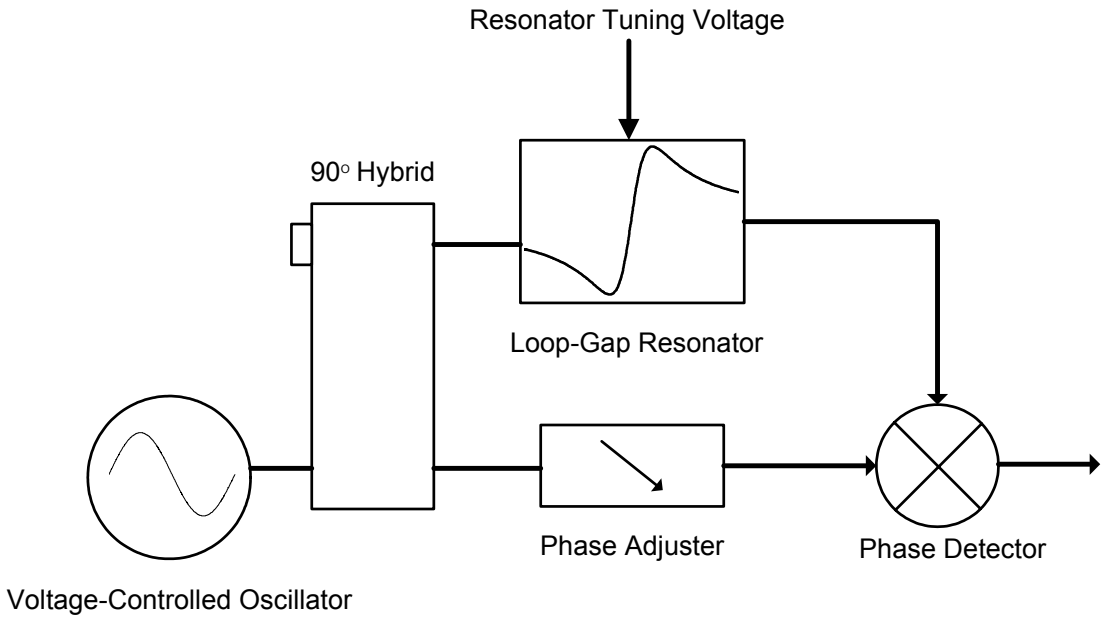

Figure 4.6: Frequency Discriminator

For an instrument, a hybrid coupler is ideal for the power divider because of high isolation between the RF and LO ports, which prevents reflected signals from circulating in the frequency discriminator. The mixer used in the prototype was a double balanced passive diode ring mixer, Mini-Circuits model JMS-5MH. The VSWR of this mixer at the LO and RF ports is approximately 2.9 in the 1000 – 1250 MHz range, equivalent to reflection magnitude $|s_{11}|$ as large as -6.3 dB. In all the measurements which follow, the RF port of

the mixer has a 6dB pad following the loop-gap resonator, not shown in Figure 4.6. The measured power variations at the RF port are shown below (Figure 4.7):

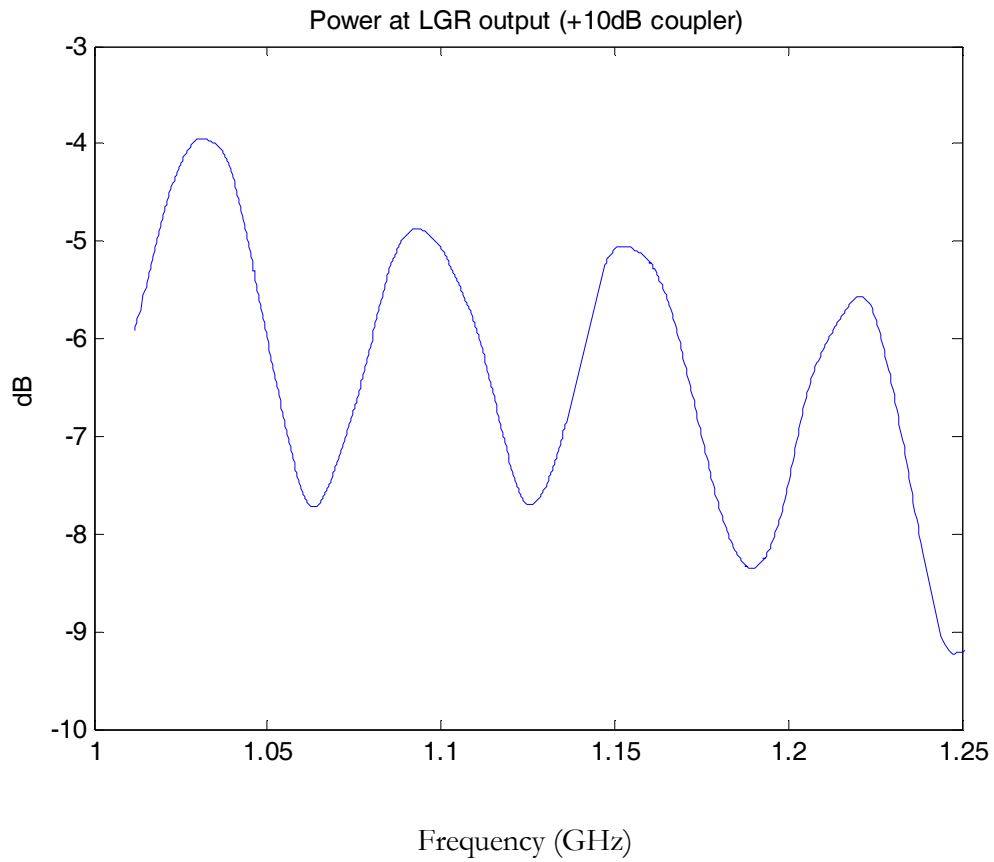

Figure 4.7: Power Variations at Mixer Input Because of Loop-Gap Resonator Mismatch

The equivalent power at the RF port of the mixer is 4 dB larger, which accounts for the 10dB directional coupler and the 6 dB pad. The 6dB pad is used to improve the matching to the mixer RF port. The power at the LO port is between 11.4 and 12.8 dBm over the same 1000 – 1250 MHz band. Measurements of the prototype resonator s-parameters show that the large power variation in Figure 4.7 is due to mismatch of the loop-gap resonator output impedance.

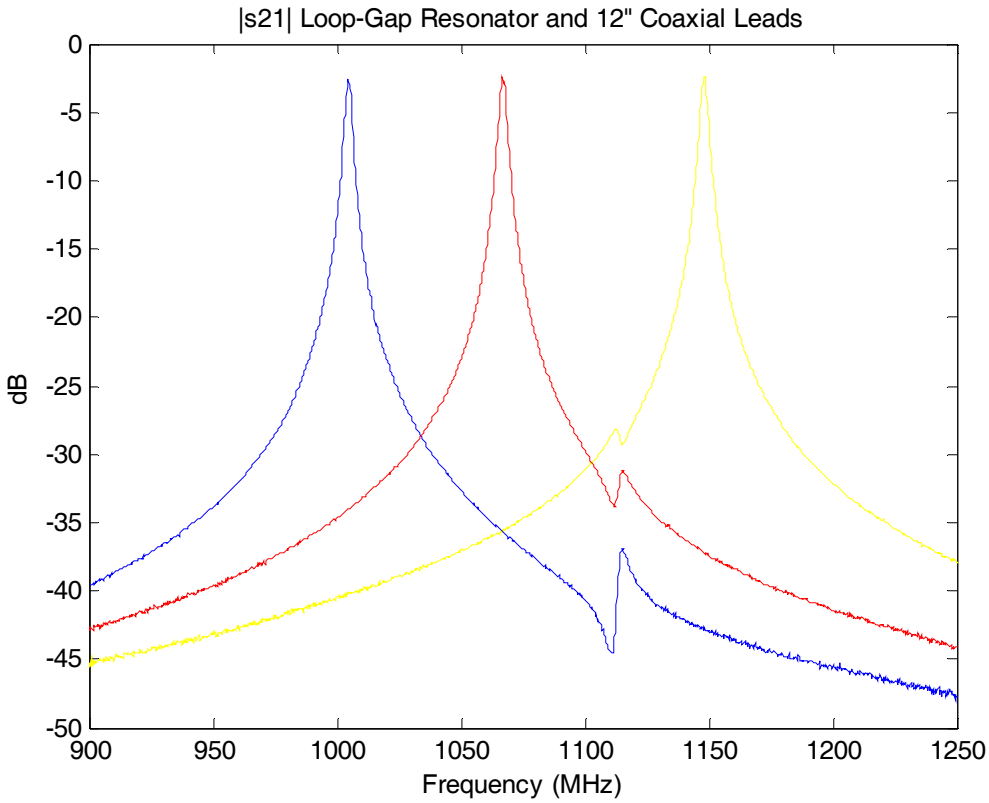

Figure 4.8 Measured Loop-Gap Resonator Transmission at 3 Frequencies

The transmission characteristics of the prototype loop-gap resonator are shown above for the resonator tuned to ~1000 MHz, 1060 MHz, and 1150 MHz (Figure 4.8).

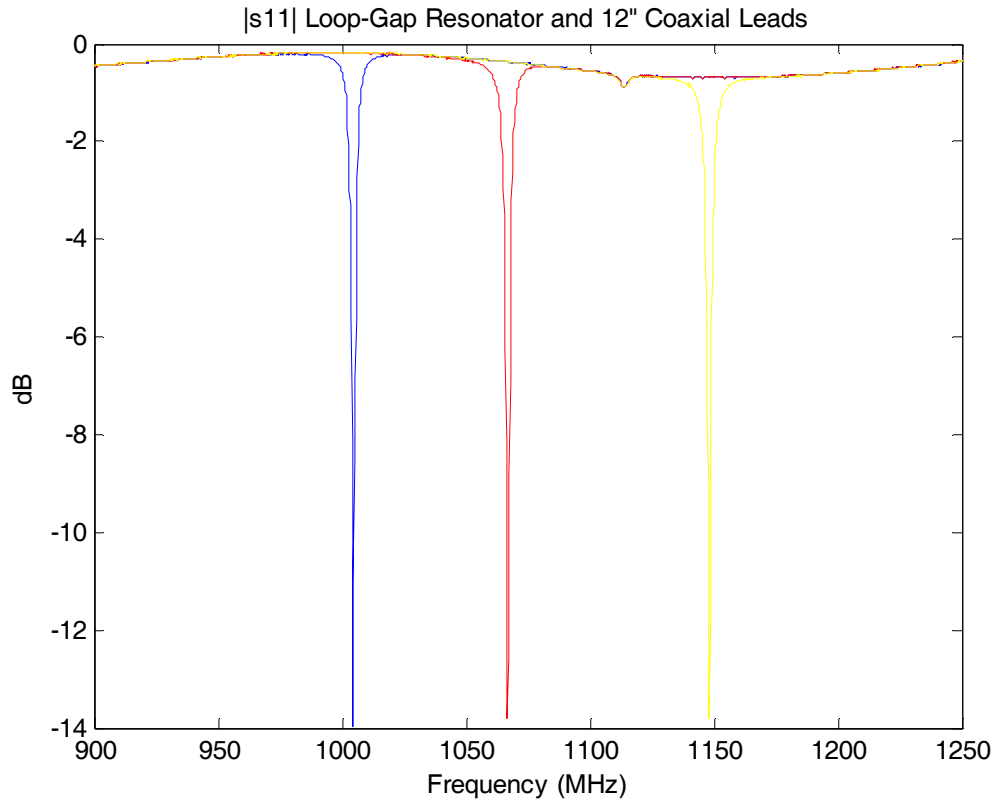

Figure 4.9 Measured Loop-Gap Resonator Reflection at 3 Frequencies

The |s11| reflection measurements are plotted above in Figure 4.9. The VSWR results from a matching problem between the output impedance of the LGR (approximately 80Ω) and the input impedance of the mixer.

A plot of VSWR near the passband is shown below, with a minimum VSWR of 1.5:

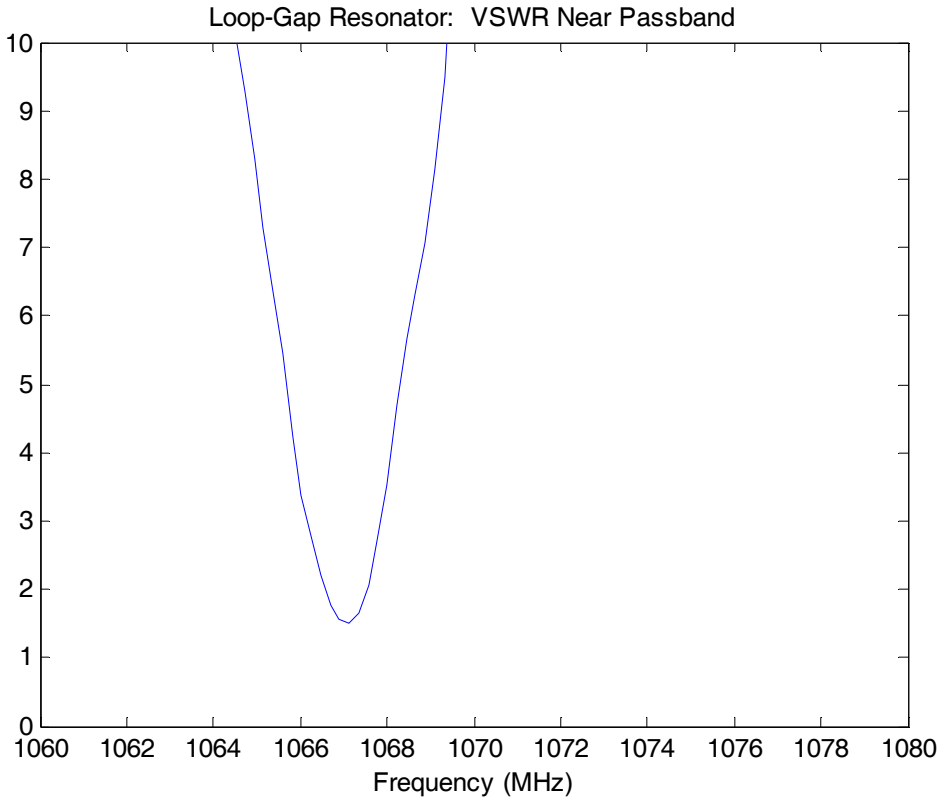

Figure 4.10 Voltage Standing Wave Ratio without Series Matching Capacitor

The VSWR of 1.5 corresponds to |s11| = -14dB, or an equivalent resistance of 75Ω. The power variations observed at the mixer would be 3.5 dB maximum in this case. The mismatched source will also cause phase variations different from the delay along the coax connecting the LGR to the mixer RF port, VSWR 1.5 corresponds to phase variations of ~ ±12º.

The matching of the loop gap resonator is greatly improved by adding a series capacitor (6.8pF ATC 600S capacitor) at the coupling loop to cancel the coupling loop series inductance, which improves matching to better than -20 dB.

The measured improvement in VSWR with the improved resonator matching and using a hybrid coupler for better isolation (Krytar 4010180) is shown in Figure 4.11, with less than 1dB power variation:

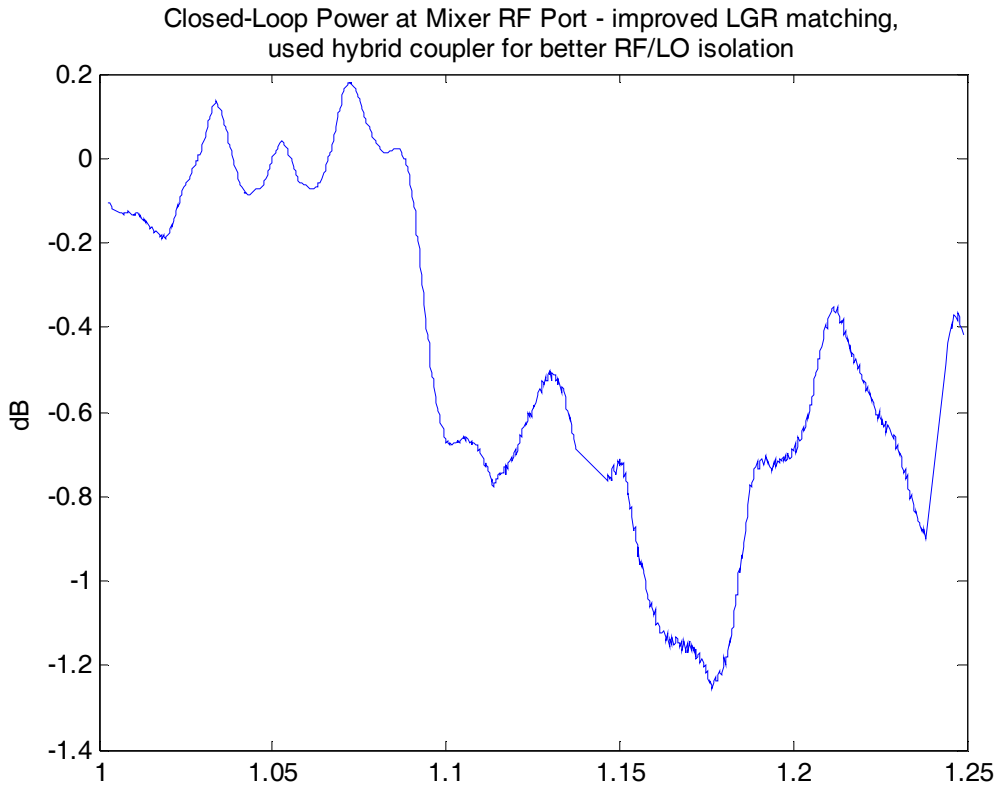

Figure 4.11 Power Variations at Mixer Input Port with Improved Resonator Matching

The power variations shown above can be compared to the much larger variations in Figure 4.7 where the matching of the loop-gap resonator is not optimized.

4.5 Automatic Frequency Control

The loop-gap resonator frequency is adjusted to track the frequency of the voltage-controlled oscillator using a simple integrator to lock the mixer input in quadrature (Figure 4.12):

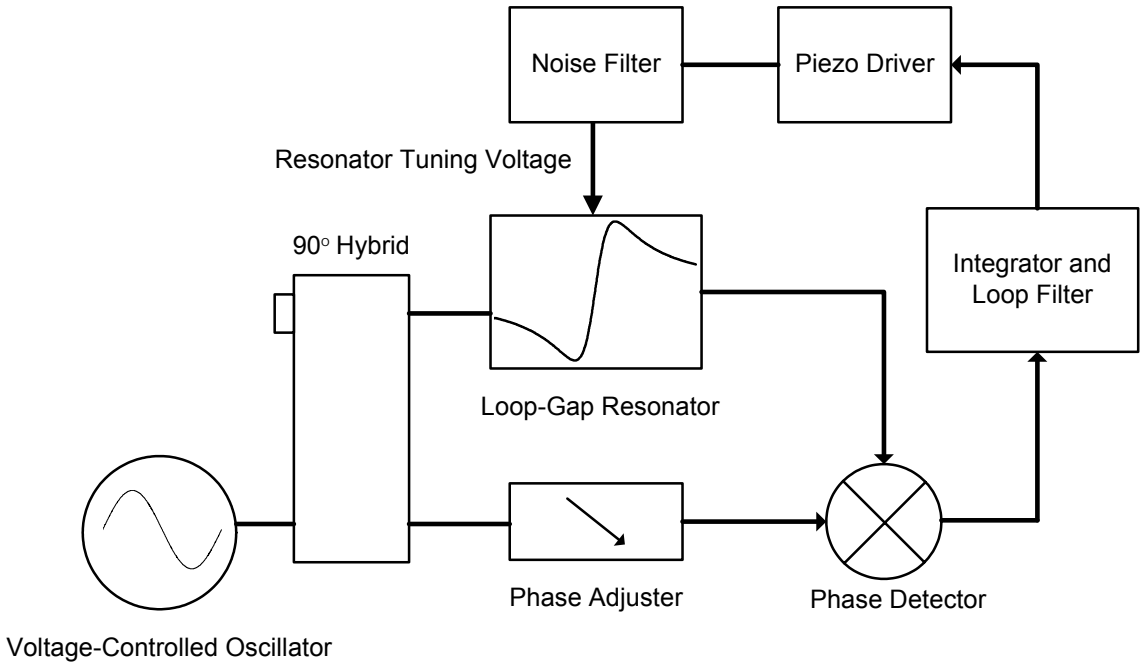

Figure 4.12 Frequency Discriminator with Automatic Frequency Control

In the prototype, the bandwidth of the loop is on the order of 1 Hz. The loop is much slower than the modulation frequency (kHz range) used to detect magnetic resonance, and therefore the frequency control does not compensate the desired signals.

4.6 Modulation Waveforms and Modulation Driver

The bidirectional waveform greatly reduces spurious pickup of the modulation waveform. Also, ac coupled audio power amplifiers may be used to process the bidirectional waveform, because the average is zero. The modulation driver needs to drive currents of several amps to an inductive load of ~ 0.25mH. For an instrument, power consumption is not a critical constraint, and the best design is to reduce the inductance of the modulation coils by using fewer turns and driving the maximum current. One driver design used an audio power op-amp (National Semiconductor LM675) and a current feedback arrangement to drive the modulation coil. The bidirectional waveform was generated from a square-wave using a divide-by-two circuit and multiplier.

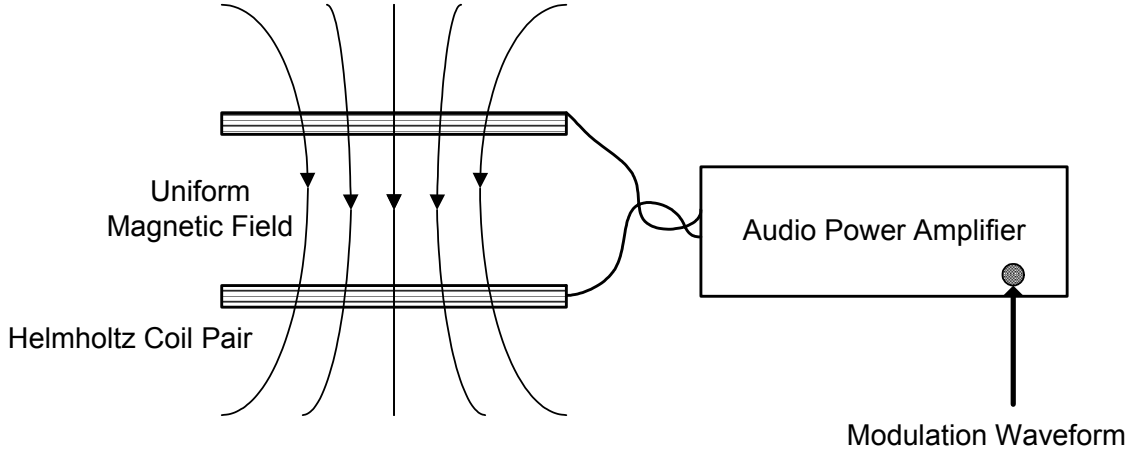

Figure 4.13: Magnetic Field Modulation

A second design uses a commercial 200W audio power amplifier (JL Audio Model 1200e monoblock full-range amplifier). The audio power amplifier is powered from a car battery, and has good linearity. The bidirectional waveform is generated using direct-digital synthesis from an arbitrary waveform generator (HP Model 33120A). The audio amplifier can drive up to 10 A at 2 Ohms. Running from a car battery is also useful in preventing large modulation currents from coupling to earth ground and common mode voltage. Another possibility is to pre-distort the audio waveform in software to adjust the driving voltage so that the current through the inductor better approximates a square wave.

4.7 Helmholtz Coil Design and Magnetic Field Homogeneity

The loop-gap resonator is place between two modulation coils, which are used to apply an audio magnetic field to the paramagnetic sample. Helmholtz coils are a pair of wire coils separated by a distance equal to the radius of the two coils. The reason Helmholtz coils are used in magnetic resonance spectrometers is because the magnetic field inside a Helmholtz coil pair is uniform over approximately 2/3 of the radius.

In the prototype spectrometer, the diameter of the coils is approximately 1.8'' inches, and the spacing of the two coils is 0.9'' inches. Each coil has approximately 30 turns and the two coils are connected in parallel. The magnetic field at the center of the coils is (in Gauss):

$$H \approx 0.9\frac{nI}{a} \tag{4.2}$$

where n is the number of turns, I is in amperes, and radius a in centimeters. For the parameters given above,

$$H \approx 0.9\frac{30I}{0.9 \cdot 2.54cm} = 11.8G/A \tag{4.3}$$

The LM675 driver circuit is limited to a peak current of approximately 2A, and if the coils are in parallel, the peak magnetic field is approximately 12 Gauss.

A typical sample of magnesium oxide used in the experiment has dimensions of roughly 1 centimeter on a side, and is placed in the center of the loop-gap resonator. The local magnetic field can be calculated from the Biot-Savart law. The magnetic field along the z-axis through the center of the coils is:

$$H = \frac{\mu_0 nI}{2}\left(\frac{a^2}{\left(5/4\,a^2 + az + z^2\right)^{3/2}} + \frac{a^2}{\left(5/4\,a^2 - az + z^2\right)^{3/2}}\right) \tag{4.4}$$

where z is the distance from the center of the coil pair, and the magnetic field is directed along the z-axis. The calculated field is plotted below (Figure 4.14), and is uniform to within 0.05 Gauss within ±0.5 cm from the center:

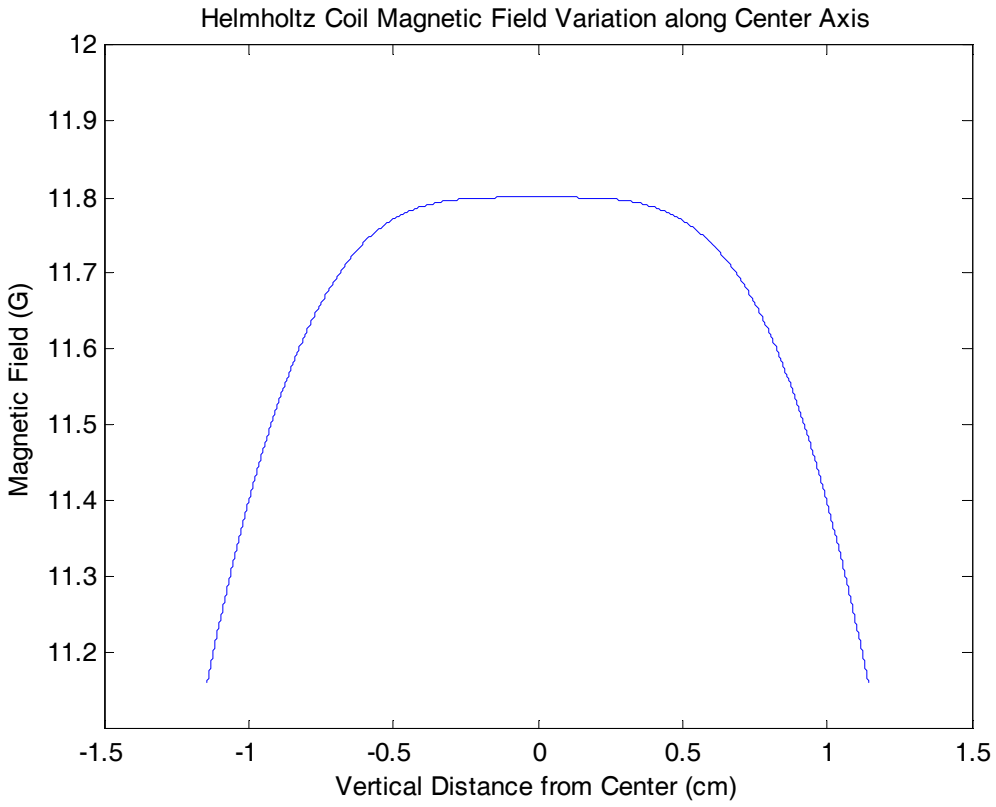

Figure 4.14 Helmholtz Coil Axial Magnetic Field Variation

The radial variation along the plane is seen to be uniform over approximately 2/3 of the radius using a similar calculation. Therefore, the modulation field at the sample is uniform to better than 1% of the peak magnetic field.

4.8 Voltage-Controlled Oscillator and Phase Noise

The voltage-controlled oscillator used in the prototype was Z-Communications, Inc. model CLV1100E. The supply and varactor node must be carefully filtered to achieve optimal phase noise performance. A measurement of the CLV1100E phase noise is shown in Figure 4.7.1, which can be compared to the phase noise output of a Hewlett-Packard Model 8665B Synthesized Signal Generator. The phase noise at 1 kHz offset from carrier is -80dBc/Hz in both cases.

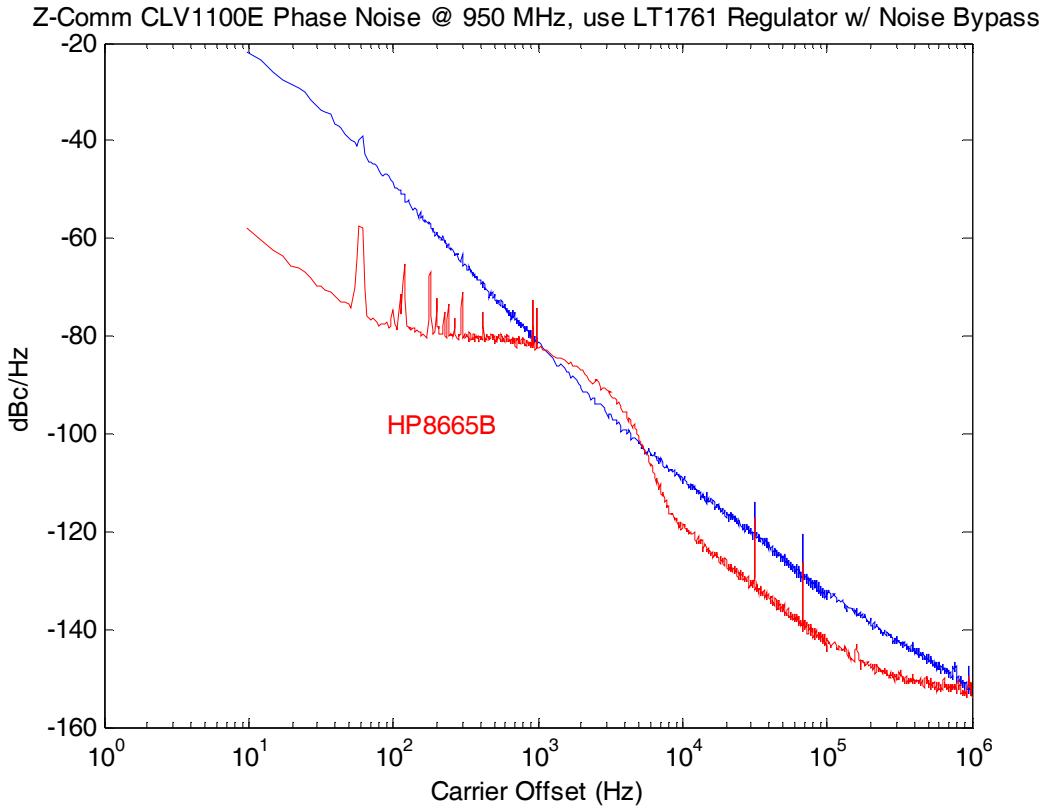

Figure 4.15 Measured Voltage-Controlled Oscillator Phase Noise

4.9 Grounding and Shielding

An important consideration in the RF system design is to prevent leakage of the RF signal to avoid unwanted modulation with the driver circuit. This is one reason why the electroplated resonator design is essential, because by using an electroplated shield, the audio modulation field penetrates the sample without attenuation, and the radio-frequency field is completely contained, since the metal thickness is several times the RF skin-depth.

Ground is also an important consideration. Isolating the large currents from the modulation driver is absolutely essential. This can be achieved by using floating differential signal inputs to the driver amplifier, which is standard practice in audio design. A good reference on grounding and shielding is the book by H. Ott [13.]

4.10 Sample Preparation and Heat Treatment

The vanadium doped magnesium oxide samples used in the experiment were signal crystal magnesium oxide grown using an arc furnace, obtained from Escete Technology (The Netherlands.) Single crystal samples are not essential, and ceramic samples can be fabricated by sintering high purity powders. The heat treatments described below were performed at Caltech using a tube furnace equipped with a gas flow controller.

In the magnesium oxide samples as grown, most of the vanadium is incorporated in the trivalent state. Heat treatment in a reducing atmosphere is essential to convert a significant fraction of the vanadium ions to the divalent state [14,15,16]. (The paramagnetic resonance spectrum of the trivalent state cannot be measured at room temperature because of the non-zero orbital angular momentum, a therefore large spin-lattice coupling.) Annealing at 1100°C in an atmosphere 4 parts argon and 1 part hydrogen is one effective recipe for

reducing the vanadium ions to the divalent state. Excessive heat treatment results in formation of a black precipitate in the magnesium oxide samples.

The X-band (*i.e.*, high-field) spectrum of a sample of magnesium oxide as grown is shown below in Figure 4.16, where the six larger lines are from the manganese ions (I = 5/2), and the eight smaller resonances are from divalent vanadium (I = 7/2):

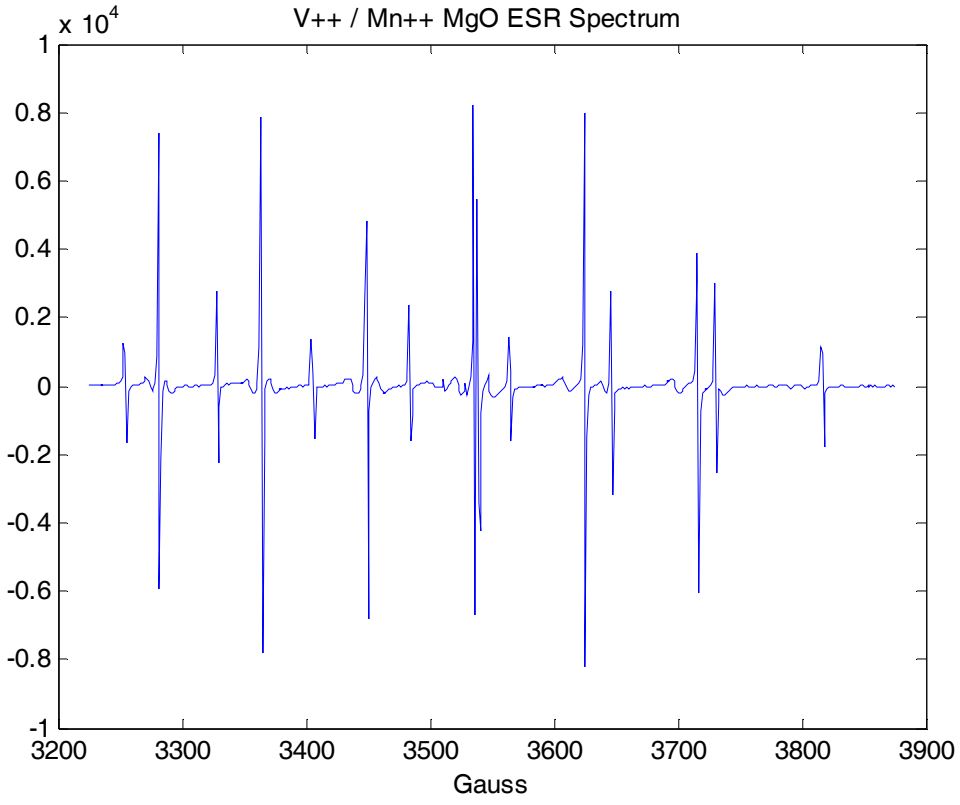

Figure. 4.16 V++/Mn++/MgO Spectrum in Samples as Grown

The spectra shown in Figures 4.16 and 4.17 were measured at Caltech using a commercial X-band ESR spectrometer. The effect of annealing the sample is shown very clearly in the next figure, where the eight lines of the vanadium spectrum are now much more intense than the manganese spectrum (Fig. 4.17). The concentration of divalent manganese ions can be taken as constant in comparing the two figures.

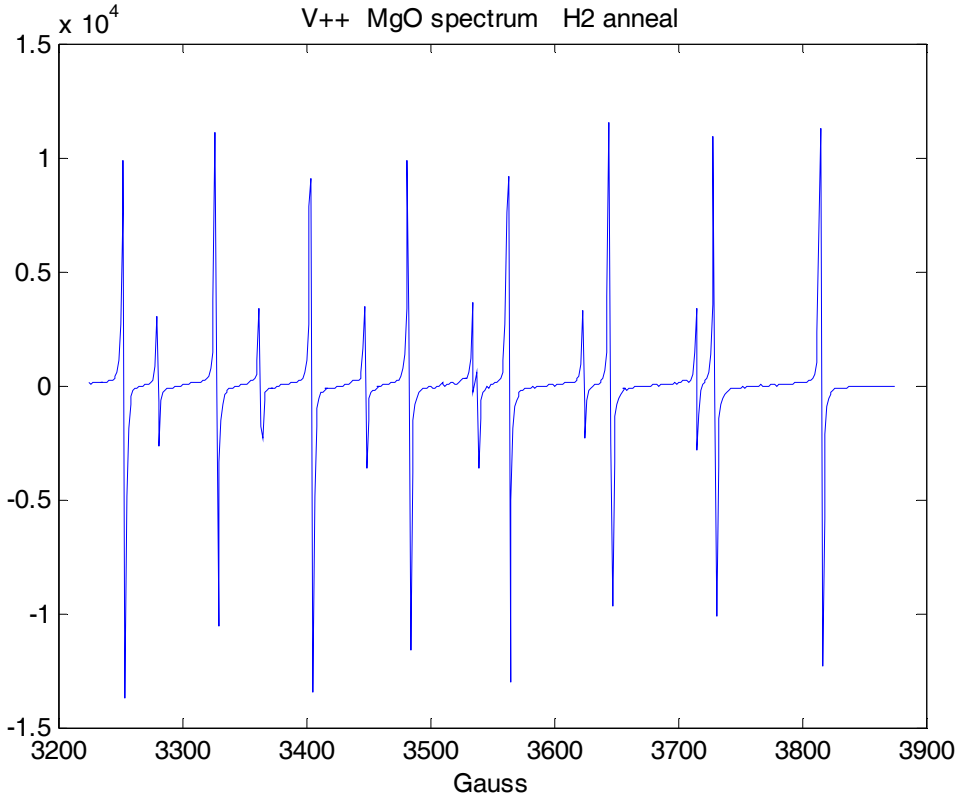

Figure 4.17 Spectrum after Annealing 6 hours @ 1100 °C in H^2/Argon Atmosphere

Given that the concentration of ions is proportional to the area under the resonance curve, we can see that the divalent vanadium concentration is increased by at least a factor of ten following heat treatment. Other possible heat treatments are discussed in the article by Wertz *et. al.* [14].

The chemistry of magnesium oxide, and the effects of various heat treatments and doping combinations can involve many factors [17,18,19,20]. Precipitates may be formed while annealing [19,20], as was observed for samples annealed for 12 hours at 1100°C, where a black precipitate is formed in the absence of oxygen. Therefore, developing a "recipe" for growing high-purity magnesium oxide ceramic containing divalent vanadium is a subject for further study.

BIBLIOGRAPHY, CHAPTER 4

[1] Christopher D. Delfs and Richard Bramley, "Zero-field Electron Magnetic Resonance Spectra of Copper Carboxylates," *J. Chem. Phys.* 107, 8840, 1997.

[2] Christopher D. Delfs, Richard Bramely, "The Zero-Field ESR Spectrum of a Copper Dimmer," *Chemical Physics Letters*, 264, 333, 1997.

[3] Richard Bramley and Steven J. Strach, "Zero-Field EPR of the Vanadyl Ion in Ammonium Sulfate," *J. of Magnetic Resonance*, 61, 245, 1985.

[4] Richard Bramley and Steven J. Strach, "Electron Paramagnetic Resonance Spectroscopy at Zero Magnetic Field," *Chem. Rev.*, 83, 49-82, 1983.

[5] Pilbrow, J.R., Troup, G. J., Tirkel, A. Z., Hutton, D. R., Gruner, L., and McLaren, N. R., United States Patent 4,803,624, "Electron Spin Resonance Spectrometer," February 7, 1989.

[6] Eugene N. Ivanov, M. E. Tobar, R. A. Woods, "Microwave Interferometry: Application to Precision Measurements and Noise Reduction Techniques," *IEEE Trans. on Ultrasonics, Ferroelectrics, and Frequency Control*, 45, 1526, 1998.

[7] Eugene N. Ivanov, Micheal E. Tobar, Richard A. Woode, "Applications of Interferometric Signal Processing to Phase-Noise Reduction in Microwave Oscillators," *IEEE Trans. on Microwave Theory and Techniques*, 46, 1537, 1998.

[8] W. Piasecki, W. Froncisz, and James S. Hyde, "Bimodal Loop-gap Resonator," *Rev. Sci. Instrum.*, 67, 1896, 1996.

[9] S. Pfenninger, W. Froncisz, J. Forrer, J. Luglia, and James S. Hyde, "General Method for Adjusting the Quality Factor of EPR Resonators," *Rev. Sci. Instrum.*, 66, 4857, 1995.

[10] T. Christides, W. Froncisz, T. Oles, James S. Hyde, "Probehead with Interchangeable Loop-gap Resonators and RF Coils for Multifrequency EPR/ENDOR," *Rev. Sci. Instrum.*, 65, 63, 1994.

[11] W. Froncisz and James S. Hyde, "The Loop-gap Resonator: A New Microwave Lumped Circuit ESR Sample Structure," *J. Magnetic Resonance*, 47, 515, 1982.

[12] W. N. Hardy and L. A. Whitehead, "Split-ring Resonator for use in Magnetic Resonance from 200-2000 MHz," *Rev. Sci. Instrum.*, 52, 213, 1981.

[13] Henry W. Ott, *Noise reduction techniques in electronic systems*, New York, Wiley 1988.

[14] John E. Wertz, John W. Orton, and P. Auzins, "Spin Resonance of Point Defects in Magnesium Oxide," *Journal of Applied Physics*, Supplement to vol. 33, no. 1, pp. 322-328, January 1962.

[15] D. H. Dickey and J. E. Drumheller, "Forbidden Hyperfine Transitions in the Electron Paramagnetic Resonance of V++ in MgO," *Physical Review*, vol. 161, no. 2, pp. 279-282, September 1967.

[16] M. D. Sturge, "Optical Spectrum of Divalent Vanadium in Octahedral Coordination," *Physical Review*, vol. 130, no. 2, pp. 639-646, April 1963.

[17] W. D. Kingery *ed.* (MIT), Structure and Properties of MgO and Al203 Ceramics, *Advances in Ceramics*, vol. 10, The American Ceramic Society, Inc., 1984.

[18] A.F. Henriksen, "Precipitation in MgO," Ph.D. Thesis, M.I.T., 1978.

[19] K.N. Woods and M.E. Fine, "Nucleation and Growth of Magnesioferrite in MgO Containing 0.9 % Fe^{3+}," *J. Am. Ceram. Soc.*, vol. 52, no. 4, pp. 186-8, 1969.

[20] W. H. Gourdin, W. D. Kingery, and J. Driear, "The Defect Structure of MgO Containing Trivalent Cation Solutes: The Oxidation-Reduction Behavior of Iron," *J. Mater. Sci.*, vol. 14, pp. 2074-82, 1979.

APPENDICIES, CHAPTER 4

Appendix I: Manufacturing Drawings for Loop-Gap Resonator

Appendix II: Contact Information for Manufacturers and Suppliers:

Loop-Gap Resonator Components:

Precision Ground Fused Silica Rods:
Rayotek Scientific, Inc.
11494 Sorrento Valley Rd., Suite J
San Diego, CA 92121
Ph: (858) 558-3671 Fax: (858) 558-6213

Custom Electroplating:
Hudson Plating Works
8740 Remmet Avenue
Canoga Park, CA 91304
Ph: (818) 709-5409 Fax: (818) 709-1045
www.hudsonplatingworks.com

Silvering Solutions:
Peacock Laboratories, Inc.
54th & Paschall Ave., Philadelphia, PA 19143
Ph: (215) 729-4400 Fax (215) 729-1380
www.peacocklabs.com
HE-300 A, B, and C
77-cleanser
93-sensitizer

Rouge (for preparing MACOR surface):
Mc-Master Carr
www.mcmaster.com
Jeweler's Rouge, Red, P/N 4783A3

MACOR® (Corning Inc., Corning, New York):
Astro Met, Inc.
9974 Springfield Pike
Cincinnati, Ohio, 45215-1425
Ph: 513-772-1242 Fax: 513-772-9080
www.astromet.com

Rexolite®:
C-LEC Plastics, Inc.
Philadelphia, Pennsylvania
Ph: (215) 708 7731 Fax: (215) 708 7728
www.rexolite.com

SMA Connectors:

Pasternack Enterprises, Inc.
PO Box 16759
Irvine, CA USA 92623-6759
Ph: (949) 261-1920 Fax (949) 261-7451
e-mail: sales@pasernack.com
www.pasternack.com
PE4122, SMA female panel mount, 4-hole, solder attachment for RG405

Flexure Stage and Piezo Driver:

Thorlabs, Inc.
435 Route 206 North
Newton, NJ 07860
Ph: 1-973-579-7227 Fax: 1-973-300-3600
E-mail: sales@thorlabs.com
www.thorlabs.com
3-Axis Flexure Stage
Single Channel Piezo Driver Model MDT694

Piezo Adjuster:

Elliot Scientific, Ltd.
3 Allied Business Center, Coldharbour Lane,
Harpenden, Herts. AL5 4UT
Ph: +44(0) 1582 766300 Fax: +44(0) 1582 766340
E-mail: sales@elliotscientific.com
MDE218 Piezo Adjuster

Frequency Discriminator RF Components:

Phaseshifter:

Advanded Technical Materials, Inc.
49 Rider Avenue, Patchoque, NY 11772
Ph: 631-289-0363 Fax: 631-289-0358
E-mail: atm@atmmicrowave.com
www.atmmicrowave.com
P/N P1603D, 90°/GHz Phaseshifter

Quadrature Hybrid:

Krytar, Inc.
1292 Anvilwood Court, Sunnyvale, CA 94089
Ph: (408) 734-5999 Fax (408) 734-3017
Toll Free: 1 (877) 734-5999 sales@krytar.com
www.krytar.com
Model 3005070 90° Hybrid Coupler

Voltage Controlled Oscillator:
Z-Communications, Inc.
9939 Via Pasar, San Diego, CA 92126
Ph: (858) 621-2700 Fax: (858) 621-2722
CLV1100E Voltage Controlled Oscillator, MINI-14S – Style Package

Frequency Mixer:
Mini-Circuit, Inc.
P.O. Box 350166, Brooklyn, New York 11235-0003
Ph: (718) 934-4500 Fax: (718) 332-4661
Distribution 800-654-7949 417-335-5935 Fax 417-335-5945
ZFM-150 Frequency Mixer, 10dBm, 2 GHz

Magnesium Oxide:

Single Crystal Vanadium Doped Magnesium Oxide:
eSCeTe Single Crystal Technology B. V.
Ir. Schiffstraat 220
NL-7500 DW Enschede
The Netherlands
Ph: +31 53 435 6146 Fax: +31 53 435 2134
escete@escete.com

Software and Equipment:

Leveled RF Power:
Hewlett Packard 8347A RF Amplifier 100 kHz – 3 GHz

Frequency Counter:
Hewlett Packard 5350A Microwave Frequency Counter

Power Meters:
Hewlett Packard 437B Power Meter
Hewlett Packard E4418B EPM Series Power Meter

Power Supply for DC Modulation Coils:
Agilent E3644A DC Power Supply

Data Acquisition Card:
DaqBoard/500™
www.iotech.com

Software:
National Instruments LabVIEW 7 Express, GPIB Interface